World Journal of Diabetes

Submit a Manuscript: https://www.f6publishing.com

World J Diabetes 2025 May 15; 16(5): 103915

DOI: 10.4239/wjd.v16.i5.103915

ISSN 1948-9358 (online)

ORIGINAL ARTICLE

Basic Study

Aucubin mitigates the elevation of microglial aerobic glycolysis and inflammation in diabetic neuropathic pain *via* aldose reductase

Xue-Zhen Zheng, Hong-Yan Yu, Ye-Ru Chen, Jian-Sheng Fang

Specialty type: Endocrinology and metabolism

Provenance and peer review: Unsolicited article; Externally peer reviewed.

Peer-review model: Single blind

Peer-review report's classification

Scientific Quality: Grade A, Grade B, Grade B, Grade C

Novelty: Grade A, Grade B, Grade B

Creativity or Innovation: Grade B, Grade B, Grade B

Scientific Significance: Grade B, Grade B, Grade C

P-Reviewer: Gaman MA; Pal B; Wu QN

Received: December 4, 2024

Revised: January 26, 2025

Accepted: February 24, 2025

Published online: May 15, 2025

Processing time: 142 Days and 1.6 Hours

Xue-Zhen Zheng, Hong-Yan Yu, Jian-Sheng Fang, Department of Anesthesiology, The First People's Hospital of Chun'an County, Hangzhou 311700, Zhejiang Province, China

Ye-Ru Chen, Department of Anaesthesiology, Sir Run Run Shaw Hospital of Zhejiang University, Hangzhou 310058, Zhejiang Province, China

Co-corresponding authors: Xue-Zhen Zheng and Jian-Sheng Fang.

Corresponding author: Xue-Zhen Zheng, MD, Department of Anesthesiology, The First People's Hospital of Chun'an County, No. 1869 Huanhu North Road, Qiandaohu Town, Chun'an County, Hangzhou 311700, Zhejiang Province, China. zhengxuezhen2024@163.com

Abstract

BACKGROUND

Treatment of diabetic neuropathy is often limited by side effects. Aucubin, an iridoid glycoside derived from natural plants, exhibits notable anti-inflammatory and antioxidant properties.

AIM

To investigate the effects of aucubin on diabetic neuropathic pain (DNP) and glycolysis and inflammation in microglia.

METHODS

Streptozotocin (STZ) was used to establish a DNP animal model. Blood glucose levels and body weight of mice were measured following STZ administration. Paw withdrawal threshold was calculated for mechanical allodynia. Paw withdrawal latency was recorded for thermal hyperalgesia. The open field test and elevated plus maze was used to assess locomotor activity and anxiety-like behavior. Western blotting was utilized for analysis of protein expression. Immunofluorescence staining was measured for morphometric analysis of microglia. Glycolysis and ATP synthesis in BV-2 cell lines were detected by metabolic extracellular flux analysis. The SwissTargetPrediction and STRING databases were used for comprehensive screening to identify potential target proteins for aucubin. The molecular docking between the possible target proteins and aucubin was investigated using Auto Dock Tool. The BV-2 cell line was transfected with lentiviral AKR1B1-shRNA to further ascertain the function of AKR1B1 in the impact of aucubin on aerobic glycolysis and inflammation during high glucose stimulation.

RESULTS
Aucubin significantly improved pain and anxiety-like behavior in STZ-induced diabetic mice and restored microglial aerobic glycolysis and inflammation. Several public databases and molecular docking studies suggested that AKR1B1, MMP2 and MMP9 are involved in the effect of aucubin on DNP. Aucubin failed to restore aerobic glycolysis and inflammation in the context of AKR1B1 deficiency.

CONCLUSION
Aucubin has potential as a therapeutic agent for alleviating DNP by inhibiting expression of AKR1B1.

Key Words: Diabetic neuropathic pain; Aucubin; Glycolysis; Aldose reductase; Microglia

Core Tip: Our research demonstrates that aucubin markedly reduces pain and anxiety-like behavior in Streptozotocin-induced diabetic mice. Furthermore, aucubin reinstates microglial aerobic glycolysis and mitigates inflammation. Utilizing the SwissTargetPrediction database, we discovered 22 prospective protein targets for aucubin concerning diabetic neuropathic pain (DNP). Analysis of protein-protein interaction networks and molecular docking experiments identified the potential role of aldose reductase (AKR1B1) to streptozotocin therapy. Aucubin does not repair aerobic glycolysis and inflammation in the setting of AKR1B1 depletion. The findings indicate that aucubin could be a potential therapeutic drug for DNP, with AKR1B1 identified as a major target.

Citation: Zheng XZ, Yu HY, Chen YR, Fang JS. Aucubin mitigates the elevation of microglial aerobic glycolysis and inflammation in diabetic neuropathic pain *via* aldose reductase. *World J Diabetes* 2025; 16(5): 103915
URL: https://www.wjgnet.com/1948-9358/full/v16/i5/103915.htm
DOI: https://dx.doi.org/10.4239/wjd.v16.i5.103915

INTRODUCTION

Diabetic neuropathy is a common complication affecting individuals with type 1 or type 2 diabetes. Approximately, 20%-50% of diabetic patients develop peripheral neuropathy[1]. Distal symmetric sensorimotor polyneuropathy (DSPN) represents the predominant form of neuropathy in individuals with type 1 or type 2 diabetes, accounting for 80%-90% of diabetic neuropathies[2]. Pain is a primary symptom of diabetic neuropathy[3,4]. The incidence of painful DSPN (P-DSPN) exhibits significant variability. Prevalence of P-DSPN from two hospital-based studies in Qatar and Libya was 34.4% and 42.2%, respectively[5]. In absolute terms, with an expected global diabetes prevalence of 472 million by 2030, diabetic peripheral neuropathy is projected to affect > 236 million individuals globally, incurring significant costs[6]. However, the mechanisms underlying the persistence of diabetic neuropathic pain (DNP) are still not fully understood. Factors such as increased activity of the polyol pathway, oxidative and nitrosative stress, microvascular impairment, altered action potentials, and microglial activation have been implicated in its pathogenesis[3]. It is widely accepted that hyperglycemia significantly contributes to the onset of this complication[4].

Metabolic reprogramming induced by hyperglycemia is a crucial factor in the development of numerous diabetes complications, such as DNP[7]. Microglia, primarily resident immune cells in the nervous system, play a crucial function in immune surveillance. In the context of inflammation, activated microglia keep consuming glucose *via* aerobic glycolysis for the production of energy, despite sufficient oxygen supply[8].

The enzyme aldose reductase catalyzes the conversion of glucose to sorbitol, utilizing NADPH in the hyperglycemia process[9]. Aldose reductase (also known as AKR1B1) serves as the rate-limiting enzyme in this pathway[10]. Studies indicate that cancer cells transform glucose into fructose *via* a mechanism involving the AKR1B1-mediated polyol pathway. The deletion of AKR1B1, which inhibits the endogenous production of fructose, significantly curtailed glycolysis[11]. Homozygosity for variants in the aldose reductase gene promoter increases the confers increased risk of neuropathy in children and adolescents with type 1 diabetes[12]. Numerous aldose reductase inhibitors (ARIs) have been developed, but many were discarded due to adverse effects and limited efficacy[13]. Among these, epalrestat has emerged as a highly promising ARI, demonstrating potential to slow down the progression of DNP and alleviate its symptoms [14,15].

In addition to glycemic control, pharmaceutical interventions for DNP mainly focus on symptomatic relief rather than addressing underlying pathophysiological mechanisms. These treatments are often limited by side effects and the potential for tolerance development[16]. Recently, pharmaceutical research has increasingly emphasized developing novel pain management therapies, particularly those incorporating dietary supplements and traditional medicinal plants.

Aucubin, an iridoid glucoside, is found in various plant species and is recognized for its anti-inflammatory, antioxidant, hepatoprotective, and neurologically protective properties[17]. Recent investigations have demonstrated that aucubin effectively inhibits activation of proinflammatory cytokines by microglia and astrocytes[18,19]. Aucubin treatment reduced 1-methyl-4-phenyl-1,2,3,6-tetrahydropyridine-induced activation of substantia nigra microglia and

astrocytes in Parkinson's disease mice[17]. Aucubin markedly reduced cerebral edema and histopathological injury, enhanced cognitive abilities, and facilitated neuronal preservation in a murine model of traumatic brain injury by reducing reactive oxygen species and inflammatory responses[20]. In this study, we established a DNP model by administering streptozotocin (STZ) intraperitoneally (intraperitoneal injection) and sucrose solution. Our objective was to investigate the effects of aucubin on DNP and glycolysis and inflammation in microglia. We identified its target protein, AKR1B1, through database searches, followed by validation of these putative targets. The findings suggest that aucubin holds promise as a therapeutic agent for downregulation that increases microglial aerobic glycolysis and inflammation in DNP by the target protein of AKR1B1.

MATERIALS AND METHODS

Animals

Adult male C57BL/6 mice, aged 6-8 weeks, were obtained and housed at Zhejiang University. The mice were maintained under controlled conditions, with a temperature of 23 ± 2 °C and a 12-hour light-dark cycle. They had unrestricted access to food and water. The study was reviewed and approved by the Zhejiang University Experimental Animal Ethics Committee Institutional Review Board (Approval No. ZJU20240012). All procedures involving animals were reviewed and approved by the Institutional Animal Care and Use Committee of the Zhejiang University Experimental Animal Ethics Committee Institutional Review Board (IACUC protocol number: 27196). Additionally, the study complied with the ARRIVE guidelines. Given the recognized gender differences in pain perception and the influence of sex hormones on pain, male mice were selected for this study. This selection ensured that animal care and use conformed to established protocols, with an emphasis on minimizing distress and reducing the number of animals.

DNP model and experimental design

STZ was used to establish a DNP animal model according to previous protocols[21,22]. Following an overnight fast, the mice were administered newly prepared STZ intraperitoneal injection at 150 mg/kg, mixed with 0.1 M citrate buffer (pH 4.5). Mice in the control group were administered an equivalent volume of citrate buffer. To mitigate the risk of fatalities associated with acute hypoglycemia, all mice received a 10% (w/v) sucrose solution for 2 days following injection of STZ. Random blood glucose levels obtained from the tail vein were measured using a glucometer (Yuyue, China). Diabetes was confirmed as a blood glucose level > 16.7 mmol/L within 72 hours following STZ administration. DNP was diagnosed when the ratio of mechanical pain threshold to baseline mechanical pain threshold was < 0.8.

To examine the antinociceptive effects of aucubin on DNP, mice were randomly allocated to four groups: Control (Con) + vehicle (Veh), Con + aucubin, STZ + Veh, and STZ + aucubin. The mice received intraperitoneal injection of aucubin (10 mg/kg) or standard saline daily for 8 consecutive days starting on day 28 following STZ administration (Figure 1). Each group contained a minimum of 12 individuals. The behavior of all mice in each group was recorded. Upon completion of the behavioral experiments, the mice in each group were randomly assigned to subsequent assays: Western blotting, real-time PCR, and immunofluorescence staining. The sample size for each experiment is specified in the figure legends.

Mechanical allodynia

Mechanical allodynia was assessed using calibrated, c von Frey filaments on the hind paw, and the up-down method was used to ascertain withdrawal thresholds, as outlined previously[23]. Mice were individually placed in chambers, and calibrated filament forces were applied to the central plantar surface of each hind paw. Paw withdrawal threshold (PWT) was then calculated.

Thermal hyperalgesia

Thermal hyperalgesia was assessed using a Hargreaves apparatus, which directs a radiant heat source at the plantar surface of the hind paw, following established protocols[24,25]. Mice were habituated to the testing environment for 1 hour. The hot plate temperature was maintained at 55 ± 2 °C. Each mouse was placed in a test chamber on a glass plate, and the paw withdrawal latency (PWL) was recorded. The procedure was repeated three times for each mouse, with a 5-min interval between tests. The mean PWL was then calculated. A maximum exposure time of 20 seconds was set to prevent tissue damage, after which the heat stimulus was automatically terminated.

Open field test

As previously mentioned, the open field test (OFT) was used to assess exploratory behavior and locomotor activity[26]. Mice were individually placed in a white plastic box (45 cm × 45 cm × 45 cm). They were allowed to explore freely for 15 minutes. After each trial, the chamber was cleaned with 75% ethanol. The ANY-maze program (Stoelting, Wood Dale, IL, United States) was used to record and analyze mouse movements.

Elevated plus maze test

Following the guidelines provided by Zhang *et al*[24,25], the elevated plus maze (EPM) test was performed. The maze comprised two open arms and two enclosed arms, raised above the floor level. Mice were positioned individually on the maze, oriented towards an open arm, and their movements were monitored and documented for 5 minutes. Following each session, the maze was sanitized using 75% ethanol. The ANY-maze program (Stoelting) was used to track and analyze mouse movements.

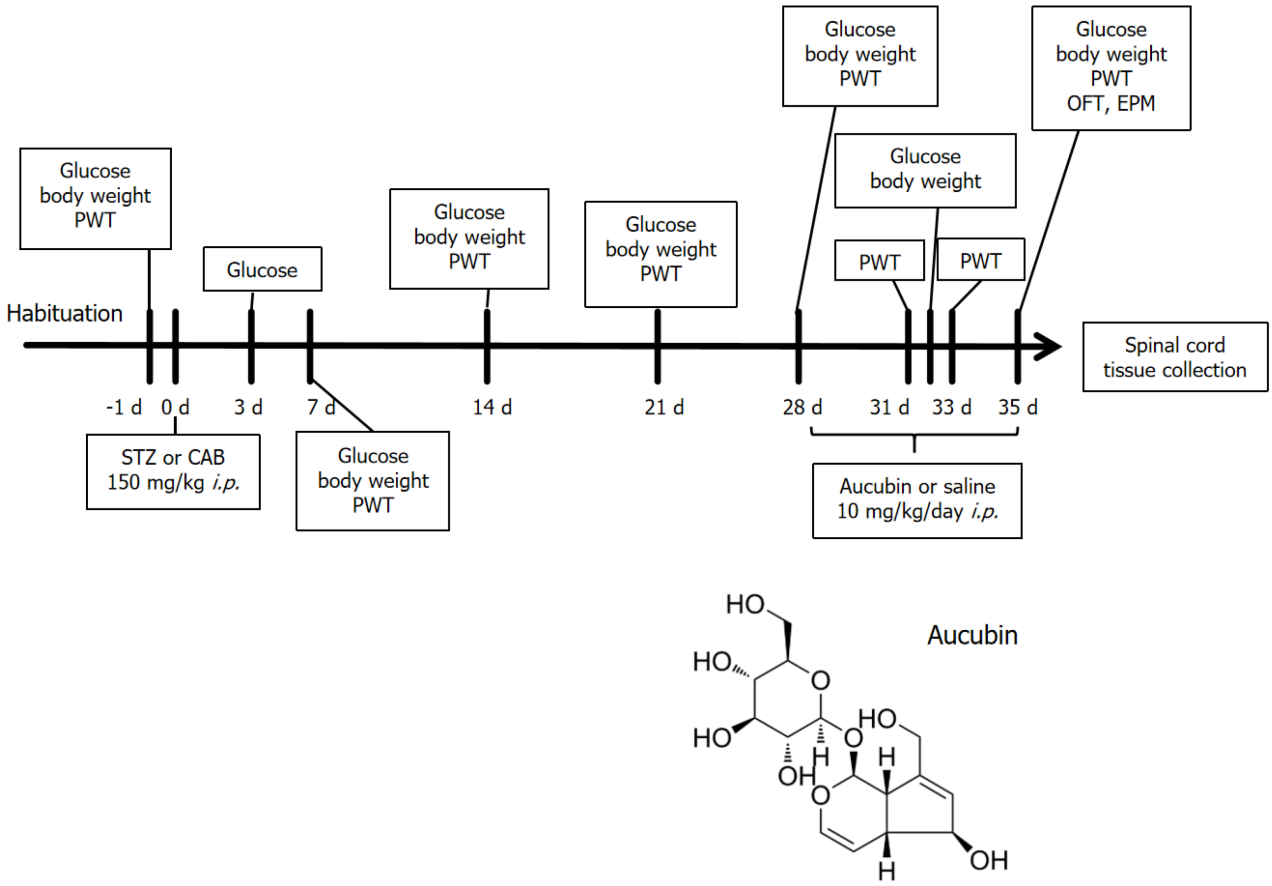

Figure 1 Schematic diagram of the experimental protocol. PWT: Paw withdrawal threshold; STZ: Streptozotocin; CAB: Citric acid buffer; *i.p.*: Intraperitoneal injection; OFT: Open field test.

Western blotting

Mice received deep anesthesia and were subsequently killed for collecting the L4-5 spinal cord segments. The tissues were homogenized in ice-cold RIPA buffer with phenylmethylsulfonyl fluoride and centrifuged at 12000 rpm for 15 minutes at 4 °C. Protein concentrations were determined using the BCA assay (Beyotime, China). Proteins were separated by SDS-PAGE and transferred to polyvinylidene difluoride membranes. Membranes were blocked with 5% nonfat milk in PBST for 1 hour at room temperature, followed by overnight incubation at 4 °C with primary antibodies: Tumour necrosis factor-α (TNF-α; 1:1000, ABclonal China, A11534); interleukin (IL)-1β (1:1000, ABclonal, A16288); IL-6 (1:1000, ABclonal, A2447); AKR1B1 (1:1000, ABclonal, A13944); MMP2 (1:1000, ABclonal, A6247); and β-actin (1:3000, ABclonal, AC026). Membranes were then incubated with appropriate secondary antibodies (goat anti-rabbit/mouse HRP) for 1 hour at room temperature. Visualization was performed using enhanced chemiluminescence, and images were captured with the ChemiDoc Touch Imaging System (BioRad, Hercules, CA, Untied States). Band intensities were quantified using ImageJ software.

Immunofluorescence staining

The immunofluorescence staining test was performed as described previously[27]. Mice were anesthetized and thereafter transcardially perfused with 0.1 M phosphate-buffered saline (PBS; pH 7.4), followed by fresh 4% paraformaldehyde (PFA; pH 7.4). Brains were swiftly excised, postfixed in 4% PFA for 24 hours, transferred to 0.1 M PBS with 0.2% sodium azide (w/v), and preserved at 4 °C until sectioning. The region was immersed in 15% sucrose for 1 day, followed by a minimum further 2 days in 30% sucrose. The brain was sectioned using a vibrating microtome. Slices from the anterior cingulate cortex (ACC) were prepared for immunohistochemical fluorescence detection of Ionized Calcium-Binding Adapter Molecule 1 (Iba1). Sections were blocked in 0.1 M PBS supplemented with 2% Triton X-100 (PBST) and 2% normal goat serum for 2 hours at ambient temperature with agitation. Subsequently, sections were incubated in PBST supplemented with 2% NGS and rabbit anti-Iba1 (1:1,000, Wako). Sections were subsequently washed three times for 10 min in PBST, incubated in PBST containing 2% normal goat serum with goat anti-chicken secondary antisera conjugated to Alexa Fluor® 594 (1:1000, Abcam, United Kingdom) for 1 hour at room temperature, washed three times for 10 minutes in PBST, and mounted on Superfrost Plus slides using Prolong Gold antifade reagent with 4′,6-diamidino-2-phenylindole (DAPI; Invitrogen, Carlsbad, CA, United States). Mounted slides were preserved at 4 °C prior to confocal imaging.

Morphometric analysis for microglia

Morphometric analysis for microglia was conducted as described previously[28]. Confocal fluorescent microscopy (Nikon

A1) yielded high-quality images with distinct cellular architecture. We used a 40 × objective to examine the target area layer by layer and recreated the cellular architecture in three dimensions using multi-plane virtual-Z mode. Each region had a minimum of 5 $Iba1^+$ cells, and 10 pictures of individual microglia were captured per mouse. The analyzed images underwent skeletonization using ImageJ skeleton analysis, and the terminal sites of microglia were quantified alongside the measurement of their longest branch length. We conducted Sholl analysis on binary pictures with Sholl analysis tools for ImageJ. The quantity of intersection sites among concentric circles was quantified to assess the complexity of cells.

BV-2 cell culture

The BV-2 cell line, acquired from OriCell (Shanghai, China), was cultured in Dulbecco's modified Eagle's medium basic (1 ×) media (Gibco, United States, C11995500BT) supplemented with 10% fetal bovine serum (EVERY GREEN, Italy, 23010702) and 1% penicillin/streptomycin (Solarbio, China) within a humidity-regulated incubator at 37 °C with 5% CO_2. The cells were grown to 80% confluence and transfected using lentivirus AKR1B1-shRNA technology (mouse AKR1B1-targeting shRNA was obtained from GenePharma, China), as described previously[14]. The cells post-transfection were evaluated using G418 (Roche, Switzerland). Cell lines exhibiting a stable knockdown of AKR1B1 were selected for further investigation.

Metabolic extracellular flux analysis

The ideal cell density was established in advance, and the experiments were conducted as previously outlined[29]. Quadruplicates or quintuplicates of BV-2 cell lines were cultured on XF-96 plates under normal glucose (25 mmol/L) or elevated glucose (75 mmol/L) conditions. At specified time intervals, microglia were rinsed and assessed in XF Running buffer A (XF assay medium, 10 mmol/L glucose, 1 mmol/L sodium pyruvate, 2 mmol/L L-glutamine) for oxygen consumption rate (OCR) measurements, or in XF Running buffer B (XF assay medium, 2 mmol/L L-glutamine) for extracellular acidification rate (ECAR) observations. Measurements were acquired in real-time under basal conditions without drug treatment and following sequential administration of various drugs: 1 μM oligomycin, 1 μM carbonyl cyanide-p-trifluoromethoxyphenylhydrazone (FCCP), 1 μM rotenone combined with 5 μM antimycin A for the MitoStress assay, or 10 mmol/L glucose, 1 μM oligomycin, and 50 mmol/L 2-deoxy-d-glucose (2-DG) for the glycolysis stress experiment. The OCR measurement under basal settings without medications indicates the basal OCR, while ECAR measurements with glucose addition denote the basal ECAR. ATP production, reflecting the peak capacity of mitochondrial respiration, was determined by the difference between the basal OCR and the maximal OCR following FCCP administration. Glycolytic reserve, indicative of cellular glycolytic capacity under energy stress, was determined by the difference between basal and peak ECAR following oligomycin administration.

Target screening

The structural information of aucubin was retrieved from the PubChem database (https://pubchem.ncbi.nlm.nih.gov/)[30]. To predict potential drug targets, SwissTargetPrediction (http://swisstargetprediction.ch/) was utilized[31]. Utilizing "diabetic neuropathic pain" as a search term, GeneCards (https://www.genecards.org/)[32] and OMIM (https://www.omim.org) were queried to gather relevant disease targets. After merging and eliminating duplicates from the obtained data, the common targets between drug and disease were determined using Venny 2.1 (https://bioinfogp.cnb.csic.es/tools/venny/). These shared targets represent the potential targets of aucubin in treating DNP.

Construction of protein-protein interaction network

The common targets were input into the STRING database (https://string-db.org)[33], with the species set to *Homo sapiens* to construct the protein-protein interaction (PPI) network of aucubin targets for DNP. Cytoscape 3.10.1[34] software, along with the MCODE plugin, was used for further analysis. The minimum score threshold (Degree Cutoff) was set to 2, the Node Score Cutoff was 0.2, and networks with a maximum connection number of 2 (K-Core) were excluded. The depth of core nodes was limited to 100.

Gene Ontology and Kyoto Encyclopedia of Genes and Genomes signaling pathway analysis

To gain insight into the functions of genes associated with aucubin treatment of DNP, Gene Ontology (GO) annotation and Kyoto Encyclopedia of Genes and Genomes (KEGG) enrichment analyses were performed using the clusterProfiler package in R software[35]. $P < 0.05$ was considered significantly enriched. Visualization of the GO and KEGG results was conducted using the ggplot2 and GOplot R[36] packages, respectively.

Molecular docking

Aucubin was used as the ligand, and the potential target proteins were designated as receptors. The 3D structures of key core targets were downloaded from the PDB database (https://www.rcsb.org/). Preprocessing of the target structures was performed using PyMOL software. The 3D structure of aucubin was downloaded in SDF format from PubChem and converted to Mol2 format using Open Babel 2.4.1. Molecular docking between aucubin and the key core targets was conducted using AutoDock Tools 1.5.7 to validate the interaction activity. The conformation with the lowest binding energy was selected for subsequent docking mode analysis, and visualization was performed using PyMOL software. Binding energy < 0 kJ/mol indicated spontaneous binding. It is generally accepted that binding energy < -5 kcal/mol indicates a good binding activity between the ligand and the receptor[37,38].

Statistical analysis

Statistical analysis was performed using GraphPad Prism 9.0 software (La Jolla, CA, United States). Group comparisons were conducted using one-way or two-way analysis of variance, followed by *post hoc* tests for multiple comparisons. Results are presented as the mean ± SE of the mean. A significance level of $P < 0.05$ was established.

RESULTS

Aucubin alleviated STZ-induced DNP and anxiety-like behavior

Adult wide type C57BL/6 mice were treated with aucubin (10 mg/kg) daily for eight consecutive days, starting on day 28 post-STZ administration (Figure 1). The blood glucose levels and body weight of the mice were measured following STZ administration. Blood glucose levels significantly increased 72 hours post-STZ injection, indicating successful induction of diabetes. Aucubin administration during the final 8 days significantly reduced blood glucose levels in the STZ + aucubin group compared to the STZ group (Figure 2A). The STZ + Veh and STZ + aucubin groups exhibited significant body weight loss compared to the controls (Figure 2B). During the acclimation periods of mice, the STZ mice exhibited elevated blood glucose levels and a reduction in weight, absent any further specific conditions. These results demonstrated that aucubin effectively reduced STZ-induced hyperglycemia.

The efficacy of aucubin in alleviating DNP was evaluated through assessments of mechanical allodynia and thermal hypersensitivity. PWT for mechanical allodynia was significantly reduced within 14 days post-STZ injection, and PWL for thermal hypersensitivity was significantly decreased within 7 d, indicating successful induction of DNP (Figure 2C and D). Aucubin significantly increased both PWT and PWL in STZ-injected mice, demonstrating its effectiveness in mitigating mechanical allodynia and thermal hypersensitivity (Figure 2C and D).

To assess anxiety-like behavior associated with chronic pain, the OFT and EPM test were performed. Neither STZ nor aucubin altered locomotor activity, as demonstrated by no significant differences in total distance traveled during the tests (Figure 2E). However, STZ-treated mice exhibited decreased central distance in the OFT compared to controls, indicating anxiety-like behavior (Figure 2F). Aucubin treatment significantly increased central distance in STZ-injected mice (Figure 2E and F). In the EPM test, the decrease in the open arms of mice entering the open arm entries can be used as an index to judge the anxiety behavior of mice[39,40]. The STZ-treated mice showed a significant reduction in open arm entries compared to the controls, while aucubin administration reversed this effect (Figure 2G and H). These findings indicated that aucubin mitigated STZ-induced anxiety-like behavior.

Aucubin alleviated STZ-induced inflammatory responses

To assess the effect of aucubin on STZ-induced inflammatory responses, we measured expression of the inflammatory markers IL-1β, IL-6 and TNF-α. Western blotting indicated that IL-1β, IL-6 and TNF-α were significantly elevated in the spinal cord in the STZ mice compared to the controls (Figure 3A and B). Aucubin treatment resulted in a significant reduction of these inflammatory cytokines in STZ-treated mice (Figure 3A and B). Expression of nuclear factor-κB (NF-κB) p65 was increased in the nucleus and decreased in the cytoplasm in STZ-treated mice. Aucubin reversed STZ-induced activation of the NF-κB p65 pathway (Figure 3C and D). These results suggested that aucubin attenuated STZ-induced inflammatory responses in the spinal cord.

Previous report identified that microglia-meditated hyperactivity of ACC^{Glu} neurons under diabetic conditions through which pain is generated[41]. We performed morphometric analysis of microglia in the ACC. The findings indicated that the increased soma size and maximum branch length in STZ mice signified microglial activation, but aucubin mitigated this activation in the ACC (Figure 3E-G). The aforementioned studies demonstrated that aucubin mitigated STZ-induced inflammatory reactions.

Aucubin reduced aerobic glycolysis and inflammation in BV-2 cells

Glycolysis offers a rapid energy source to fulfill the requirements of microglial proliferation, polarization, chemotaxis, and other functions during inflammatory reactions[42]. We investigated the impact of aucubin on glycolysis and ATP synthesis in the BV-2 cell line. Aucubin reduced elevated mRNA levels of TNF-α, IL-1β and IL-6, which were induced by high glucose, in relation to the inflammatory response (Figure 4A). We evaluated the ECAR and OCR in the BV-2 cell line subjected to different glucose concentrations. The levels of basal glycolysis and glycolytic reserve increased in response to increasing glucose levels (Figure 4B and C). Conversely, the BV-2 cell line subjected to elevated glucose concentrations exhibited a more pronounced reduction in baseline and maximal OCR and ATP production, relative to those treated with normal glucose concentrations (Figure 4B and C). The data demonstrated that high glucose levels augmented inflammation by promoting aerobic glycolysis in microglia. Aucubin significantly diminished the basal glycolysis and glycolytic reserve stimulated by elevated glucose levels and reinstated the decline in basal and maximal OCR and ATP generation (Figure 4D and E). These data demonstrated that aucubin reduced glycolysis and inflammation in microglia under high glucose stimulation.

Potential target proteins of aucubin in DNP

To find the potential target proteins of aucubin in DNP, we utilized the SwissTargetPrediction database to comprehensively screen 100 potential target proteins. Concurrently, an extensive search of the GeneCards and OMIM databases yielded 1028 proteins associated with DNP. After removing duplicates, the intersection of these datasets was visualized using a Venn diagram, revealing 22 candidate target proteins common to both sets (Figure 5A). These proteins were

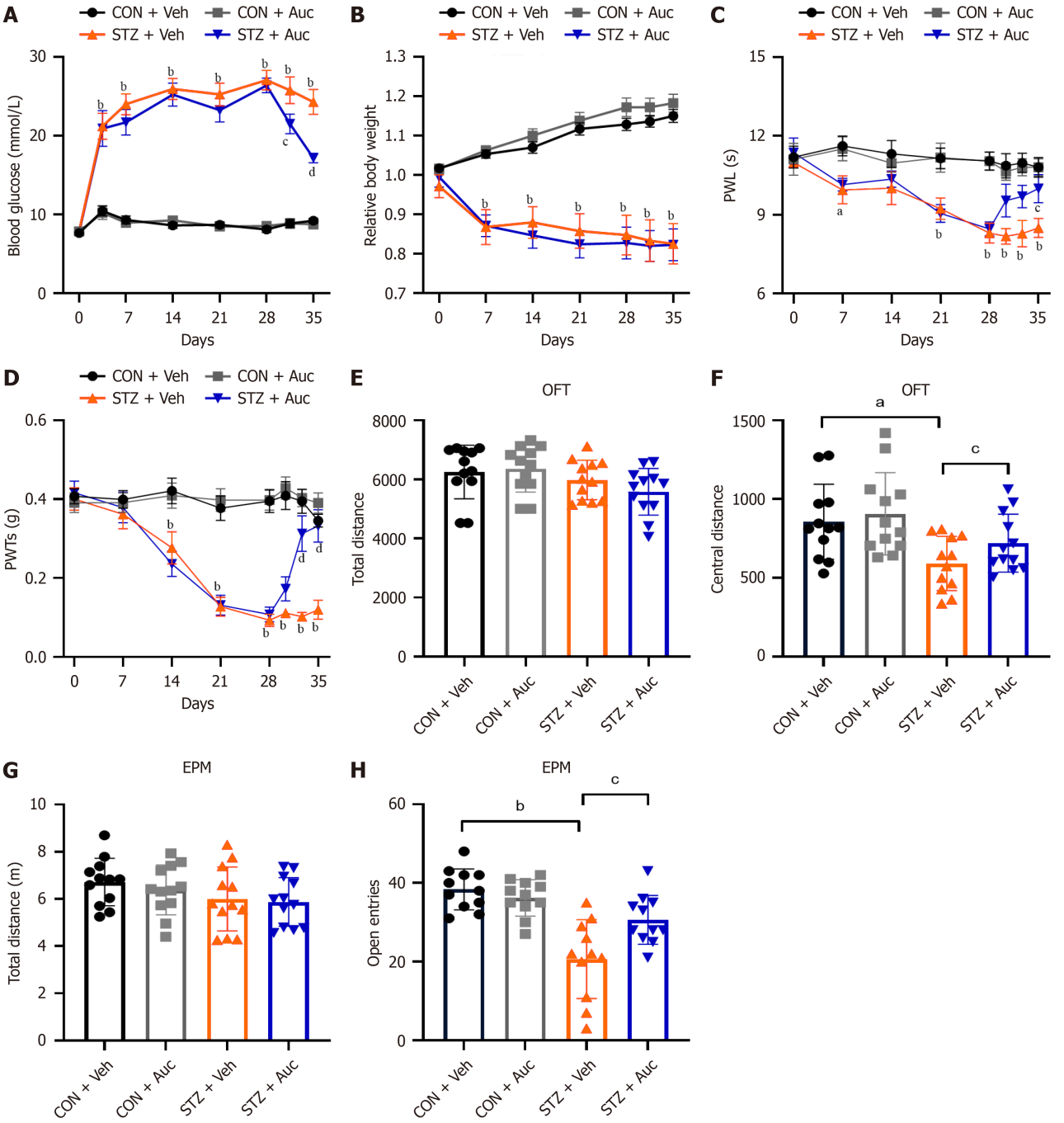

Figure 2 Aucubin alleviate streptozotocin-induced diabetic neuropathic pain and anxiety-like behavior. A: Blood glucose level of the diabetic neuropathic pain diabetic neuropathic pain (DNP): Mice after aucubin treatment; B: Body weight of the DNP mice after aucubin treatment; C: Mechanical paw withdrawal threshold in mice; D: Thermal paw withdrawal latency in mice; E: Total distance traveled in the open field test (OFT); F: Distance traveled by mice in the central area in the OFT after streptozotocin streptozotocin (STZ): Injection; G: Total distance traveled in the elevated plus maze (EPM); H: Number of entries of mice into the open arms in the EPM after STZ injection. Data are presented as means ± SEM (n = 10). $^{a}P < 0.05$, $^{b}P < 0.01$ control (CON) + vehicle (Veh) *vs* STZ + Veh; $^{c}P < 0.05$, dP < 0.01 STZ + Veh *vs* STZ + aucubin. CON: Control; STZ: Streptozotocin; Veh: Vehicle; Auc: Aucubin; PWT: Paw withdrawal threshold; OFT: Open field test; EPM: Elevated plus maze.

posited as potential targets of aucubin for alleviating DNP. The KEGG pathway analysis of the 22 candidate proteins identified their enrichment in 20 signaling pathways, using a significance threshold of $P < 0.05$. The eight most prominent pathways were selected for detailed visualization (Figure 5B), highlighting that these key pathways may be involved in the potential therapeutic effects of aucubin, notably those related to galactose metabolism. The GO analysis of the 22 target proteins revealed significant enrichment in various biological processes (BP), cellular components (CC), and molecular functions (MF). A total of 72 BP terms were significantly enriched ($P < 0.05$), encompassing cell signaling, metabolic processes, cell proliferation and differentiation, inflammation, and immune responses. We identified 22 significantly enriched CC terms ($P < 0.05$), primarily related to components of the nervous system, cell membranes, and extracellular structures. Twelve MF terms were significantly enriched, including protein and carbohydrate hydrolysis activities (*e.g.*, peptidases, endopeptidases and α-1,4-glucosidase), as well as interactions with ions (zinc ion binding),

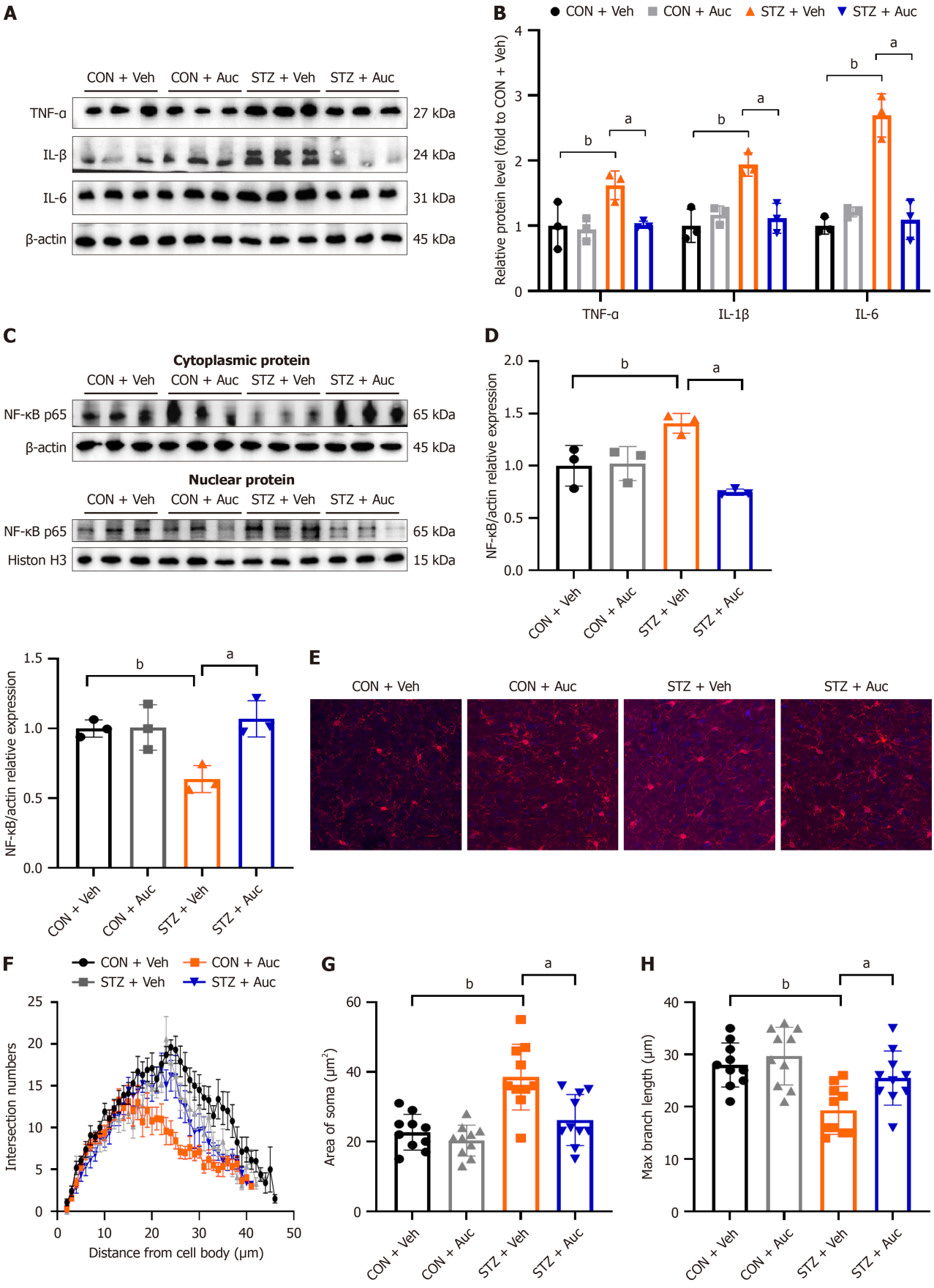

Figure 3 Aucubin releases streptozotocin-induced inflammatory responses. A: Representative bands of tumour necrosis factor-α (TNF-α), interleukin (IL)-1β, and IL-6; B; Quantitative analysis of the relative expression of TNF-α, IL-1β, and IL-6 (n = 3); C: Representative bands of nuclear factor-κB (NF-κB) in cytoplasmic protein and nuclear protein; D: Quantitative analysis of the relative expression of NF-kappa B in cytoplasmic protein and nuclear protein (n = 3); E: Representative images of immunofluorescence of iba1; F-H: Sholl analysis of microglia of interscetion numbers (F); area of soma (G); and max branch length (H).

Data are expressed as mean ± SEM. [a]*P* < 0.01 streptozotocin (STZ) + vehicle (Veh) *vs* STZ + aucubin; [b]*P* < 0.01 control + Veh *vs* STZ + Veh. CON: Control; STZ: Streptozotocin; Veh: Vehicle; Auc: Aucubin; TNF-α: Tumour necrosis factor-α; IL: Interleukin.

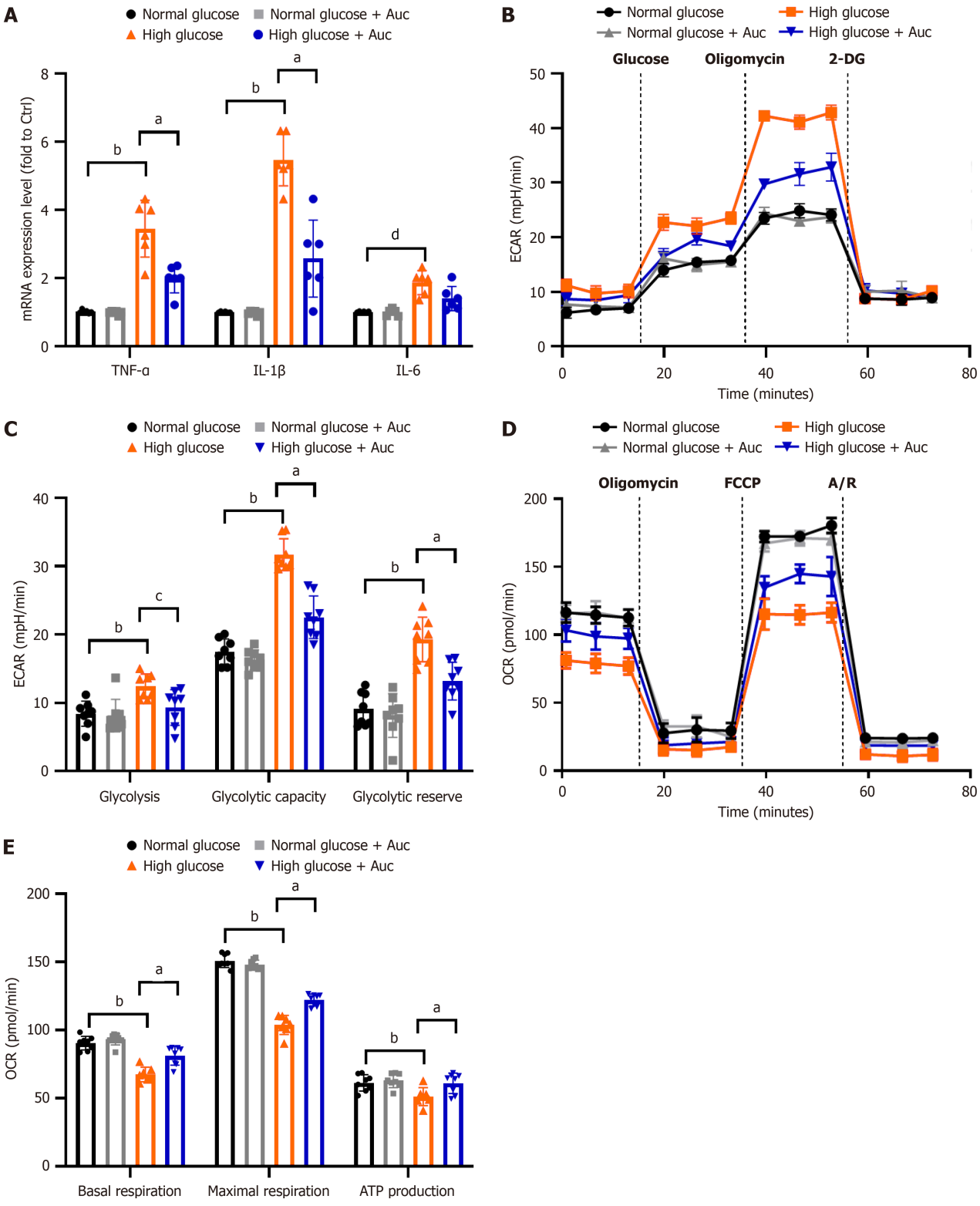

Figure 4 Aucubin reduced aerobic glycolysis and inflammation in the BV-2 cell. A: the mRNA levels of pro-inflammatory cytokine; B-E: The experimental program of the extracellular acidification rate (B and C) and oxygen consumption rate (D and E) of BV-2 measured by Seahorse XFe96 Extracellular Flux Analyzer. Data are expressed as mean ± SEM. *n* = 6. [a]*P* < 0.01 high glucose vs high glucose + auccubin (Auc); [b]*P* < 0.01 normal glucose *vs* high glucose; [c]*P* < 0.05 high glucose *vs* high glucose + Auc; [d]*P* < 0.05 normal glucose *vs* high glucose. ECAR: Extracellular acidification rate; 2-DG: 2-deoxy-d-glucose; OCR: Oxygen consumption rate; FCCP: Carbonyl cyanide-p-trifluoromethoxyphenylhydrazone; Auc: Aucubin; TNF-α: Tumour necrosis factor-α; IL: Interleukin.

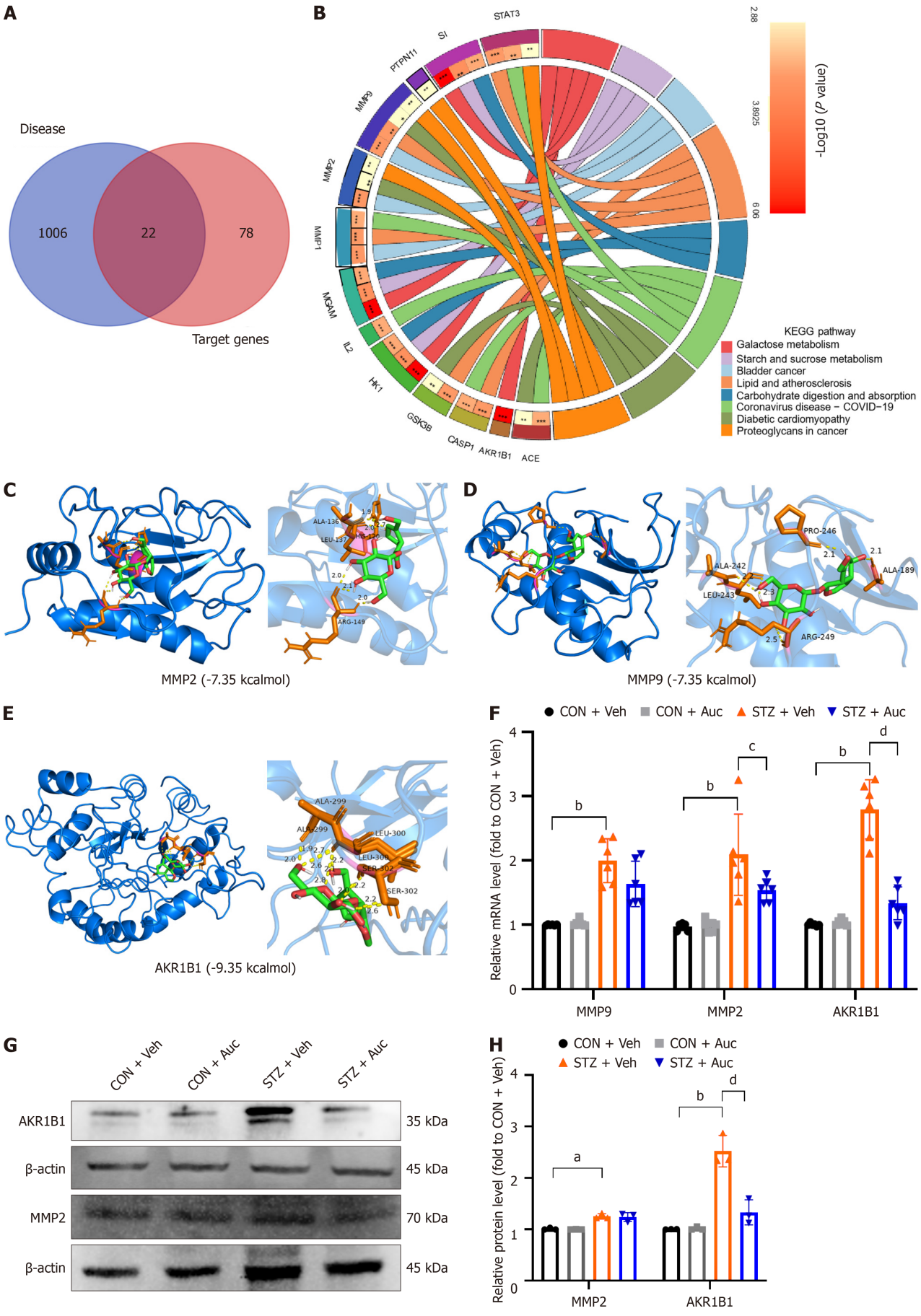

Figure 5 The potential target proteins of aucubin on the diabetic neuropathic pain. A: Venn diagram showing the potential target genes for aucubin in treating diabetic neuropathic pain; B: Kyoto Encyclopedia of Genes and Genomes pathway analysis of the potential target genes; C-E: Molecular docking between

the target 3 proteins (MMP2, MMP9, and AKR1B1) and aucubin (Auc) conducted using Auto Dock Tool 1.5.7; F: mRNA levels of MMP9, MMP2, and AKR1B1 in mice after streptozotocin (STZ) and Auc treatment. (n = 6); G: Representative bands of Western blot for MMP2 and AKR1B1 in mice after STZ and Auc treatment; H: Quantitative analysis of the relative expression of MMP2 and AKR1B1 (n = 3). Data are expressed as mean ± SEM. $^{a}P < 0.05$, $^{b}P < 0.01$ CON + vehicle (Veh) *vs* STZ + Veh; $^{c}P < 0.05$, $^{d}P < 0.01$ STZ +Veh *vs* STZ + Auc. CON: Control; STZ: Streptozotocin; Auc: Aucubin; Veh: Vehicle.

small molecules (G protein-coupled adenosine receptor activity), proteins (calcium ion binding, protein homodimerization), and carbohydrates (carbohydrate binding). Supplementary Figure 1A illustrates the top eight terms in BP, CC and MF categories based on their *P* values.

To elucidate the interactions among the 22 putative target proteins of aucubin, we used the STRING database. This refined our list to 19 proteins, which were then used to construct a PPI network (Supplementary Figure 1B). In this network, the size of each node indicates the degree of interaction, highlighting the extensive connectivity among these genes. Using the mcode plugin in Cytoscape 3.10.1, we identified key subnetworks within the PPI network. Supplementary Figure 1C shows these subnetworks, which comprised 10 genes: *SI*, *ACE*, *AKR1B1*, *HK1*, *MGAM*, *IL2*, *MMP1*, *MMP2*, *MMP9* and *STAT3*.

The molecular docking between the possible target proteins and aucubin was investigated using Auto Dock Tool 1.5.7, based on the findings from the PPI network analysis. The docking findings were imported into PyMol for visualization, displaying the hydrogen bonds between the 10 proteins and the amino acids of aucubin. The binding energy of potential targets and contacts are listed in Table 1. It is generally accepted that binding energy < -5 kcal/mol indicates good binding activity between ligands and receptors[37,38].

According to the binding energy, MMP2, MMP9 and AKR1B1, demonstrated strong binding affinity with aucubin (Figure 5C-E). Aucubin interacted with the key residues for activity and potency of these proteins, suggesting inhibition of the activity of these proteins. The target proteins with the highest binding energy were MMP2, MMP9 and AKR1B1. Multiple hydrogen bonding interactions were found between the amino acid active groups of MMP2 and aucubin. Hydrogen bonds were observed to be established at ALA-136, LEU-137 and HIS-120. MMP9 and aucubin formed hydrogen bonds with ALA-242, LEU-243, PRO-246, ALA-189 and ARG-249. AKR1B1 and aucubin formed hydrogen bonds with ALA-299, LEU-300 and SER-302.

To validate the role of AKR1B1, MMP2 and MMP9 in the effect of aucubin on STZ-induced DNP, we conducted RT-PCR and western blotting. RT-PCR indicated a significant increase in the mRNA levels of AKR1B1, MMP2 and MMP9 in STZ-treated mice (Figure 5F). Aucubin treatment ameliorated the mRNA levels of AKR1B1 and MMP2 post-STZ therapy (Figure 5F). Western blotting confirmed increased expression of AKR1B1 and MMP2 in STZ-treated mice, with aucubin significantly suppressing AKR1B1 expression (Figure 5G and H). These findings suggested that AKR1B1 was a primary molecular target of aucubin in managing DNP.

Aucubin failed to restore aerobic glycolysis and inflammation in the context of AKR1B1 deficiency

To ascertain the function of AKR1B1 in the impact of aucubin on aerobic glycolysis and inflammation during high glucose stimulation, the BV-2 cell line was transfected with lentiviral AKR1B1-shRNA. Western blotting indicated effective transfection of lentivirus AKR1B1-shRNA (Figure 6A). Aucubin reduced the production of TNF-α and IL-1β cytokines generated by elevated glucose levels (Figure 6B). Aucubin, however, did not restore inflammation in the BV-2 cell line transfected with AKR1B1-shRNA lentivirus (Figure 6B). ECAR and OCR were utilized to evaluate the glycolytic and oxidative metabolism in BV-2 cells. Aucubin reduced glycolysis in microglia under high glucose stimulation. In the context of AKR1B1 Loss, aucubin failed to restore basal glycolysis and glycolytic reserve in ECAR (Figure 6C and D) and did not reinstate basal maximal OCR and ATP generation in OCR experiments (Figure 6E and F). The data suggested that AKR1B1 served as a principal molecular target of aucubin in relation to aerobic glycolysis and inflammation in DNP.

DISCUSSION

This study aimed to clarify the effects and possible targets of aucubin on DNP caused by STZ. Our research demonstrated that aucubin markedly reduced pain and anxiety-like behavior in STZ-induced diabetic mice. Furthermore, aucubin reinstated microglial aerobic glycolysis and mitigated inflammation. Utilizing the SwissTargetPrediction database, we discovered 22 prospective protein targets for aucubin related to DNP. Analysis of PPI networks and molecular docking experiments identified the principal targets. Western blotting demonstrated an elevated expression of AKR1B1 subsequent to STZ therapy. Aucubin did not repair aerobic glycolysis and inflammation in the setting of AKR1B1 depletion. The findings indicate that aucubin could be a potential therapeutic drug for DNP, with AKR1B1 identified as a major target.

Various animal models have been used to investigate the underlying mechanisms of DNP. Commonly used models include STZ-induced rat and mouse models, chemically and nutritionally induced models, type 1 insulinopenic BB/Wor rats, type 2 hyperinsulinemic diabetic BBZDR/Wor rats, Zucker diabetic fatty rats, and transgenic/knock-out models [43]. STZ, a nitrosourea analog (2-deoxy-2(3-methyl-3-nitrosoureido)-D-glucopyranose), induces toxicity by damaging the DNA of pancreatic β-cells, leading to insulin deficiency[44]. Its similarity to glucose allows it to be transported *via* the GLUT2 glucose transporter. The susceptibility to STZ varies among animals based on age, species and strain[43]. In this study, we used intraperitoneal injection of 150 mg/kg STZ to induce DNP in mice. Within 72 hours, most mice developed hyperglycemia and experienced weight loss, consistent with previous reports[45].

Table 1 The binding energy of potential targets and contacts (kcal/mol)

Potential targets	Affinity (kcal/mol)	Contacts
ACE	-4.37	ALA-356 ASP-358
MMP2	-7.35	ALA-136 LEU-137 HIS-120 ARG-149
MMP9	-7.35	ALA-189 PRO-246 ALA-242 LEU-243 ARG-249
SI	-3.09	GLU-687 ARG-682 ILE-763 ASP-796 GLU-678
AKR1B1	-9.35	ALA-299 LEU-300 SER-302
MGAM	-4.64	CYS-15 PHE-161 ASN-71
HK1	-2.22	ASP-648
MMP1	-5.5	GLU-135 LYS-151 PHE-149 SER-142
IL-2	-4.43	GLU-60 ASN-90 SER-87 GLU-67
STAT3	-2.78	TYR-686 LYS-573 ALA-578 LEU-577 LEU-579

We assessed STZ-induced pain by measuring mechanical allodynia and thermal hypersensitivity. Aucubin (10 mg/kg) was administered for eight consecutive days, starting on day 28 post-STZ injection. Aucubin reduced elevated glucose levels, PWT and PWL induced by STZ. Additionally, STZ-treated mice showed reduced movement in the central area of an OFT, indicative of anxiety-like behavior. Aucubin treatment mitigated this anxiety-like behavior, further supporting its therapeutic potential.

Aucubin, chemically known as 1,4a,5,7a-Tetrahydro-5-hydroxy-7-hydroxymethylcyclopenta(c)pyran-1-yl-beta-D-glucopyranoside, is an iridoid glycoside frequently found in traditional medicinal plants[46]. It exhibits diverse pharmacological properties, including antioxidant, anti-inflammatory, antitumor, hepatoprotective, neuroprotective and osteoprotective effects[46]. Research has demonstrated that aucubin can prevent P12 cell damage through its ability to block mitochondrial-mediated necrosis and balancing endogenous oxidant-antioxidant levels[47]. Aucubin has been shown to inhibit the activation of astrocytes and microglia, reducing the production of proinflammatory cytokines such as TNF-α, IL-1β and high mobility group box 1 in epilepsy models[48]. Aucubin significantly mitigates neuronal death in the CA1 region of the hippocampus, thereby enhancing working memory in diabetic encephalopathy models[49,50].

Glycolysis plays a pivotal role in regulating neuroinflammation, with data suggesting that microglia can transition from mitochondrial oxidative phosphorylation to aerobic glycolysis under stress conditions[29]. Numerous investigations have established that the glycolysis product might augment the microglial secretion of proinflammatory cytokines, such as IL-6, TNF-α and IL-1β. The reduction of pain and neuroinflammation by the glycolysis inhibitor 2-DG reinforces the association between glycolysis and DNP pathogenesis. Our results in BV-2 cell line cultures indicated that aucubin reinstated microglial aerobic glycolysis and inflammation in high glucose environments. These *in vitro* data augment our *in vivo* findings, emphasizing the impact of aucubin on neuroinflammation and metabolic alterations in DNP. Despite these findings, the mechanisms by which aucubin exerts its effects on neuroinflammation and metabolic shifts associated with DNP remain unclear. This study aimed to elucidate these mechanisms by identifying proteins associated with aucubin through extensive database searches. GO and PPI analyses suggested that galactose metabolism plays a significant role in the physiological effects of aucubin on DNP. Galactose is crucial in human metabolism, particularly in energy transport and the galactosylation of complex molecules[51]. Clinical studies have shown a strong correlation between DNP and galactose metabolism[52]. Animal models of galactose poisoning exhibit increased polyol pathway activity, leading to neuropathy resembling human diabetic neuropathy, which can be mitigated by aldose reductase inhibition[53]. Further evidence suggests that polyol metabolism, influenced by the *AKR1B1* gene, is involved in diabetic neuropathy. Young individuals with type 1 diabetes often show impaired indicators of peripheral and autonomic neuropathy linked to homozygous *AKR1B1* polymorphisms. Parameters such as pupillary dilation, vibration sensation thresholds, nerve conduction studies, and postural blood pressure tests correlate with *AKR1B1* gene variants[12]. Patients with painful diabetic neuropathy exhibit significant alterations in exon 1 of the *AKR1B1* gene[54]. In this study, we observed that STZ treatment increased both mRNA levels and expression of AKR1B1. Aucubin normalized this elevated expression. To verify the role of AKR1B1 in the effect of aucubin on aerobic glycolysis and inflammation upon high glucose stimulation, the BV-2 cell line was transfected with AKR1B1-shRNA lentivirus. In the context of AKR1B1 deficiency, aucubin did not restore the levels of basal glycolysis and glycolytic reserve in ECAR and did not restore the basal, maximal OCR and ATP production in OCR assays. These findings highlight the potential role of AKR1B1 as a therapeutic target for aucubin on aerobic glycolysis and inflammation in DNP.

PPI network and molecular docking analyses suggest that the effects of aucubin on DNP may be mediated by MMP2 and MMP9. MMPs are zinc-dependent endopeptidases crucial for extracellular matrix (ECM) remodeling[55]. Pathological conditions can lead to abnormal MMP activity, causing ECM disturbances. Hyperglycemia, a key feature of diabetes, induces oxidative stress and inflammation, elevating MMP expression in both central and peripheral nervous systems[56]. These MMP-induced ECM changes increase the sensitivity of peripheral and central nerves, contributing to DNP[56]. Recent research has shown that reversing allodynia is possible through the administration of endogenous MMP-9 and MMP-2 inhibitors following peripheral nerve injury, although the effect is temporary, lasting only 3-24 hours

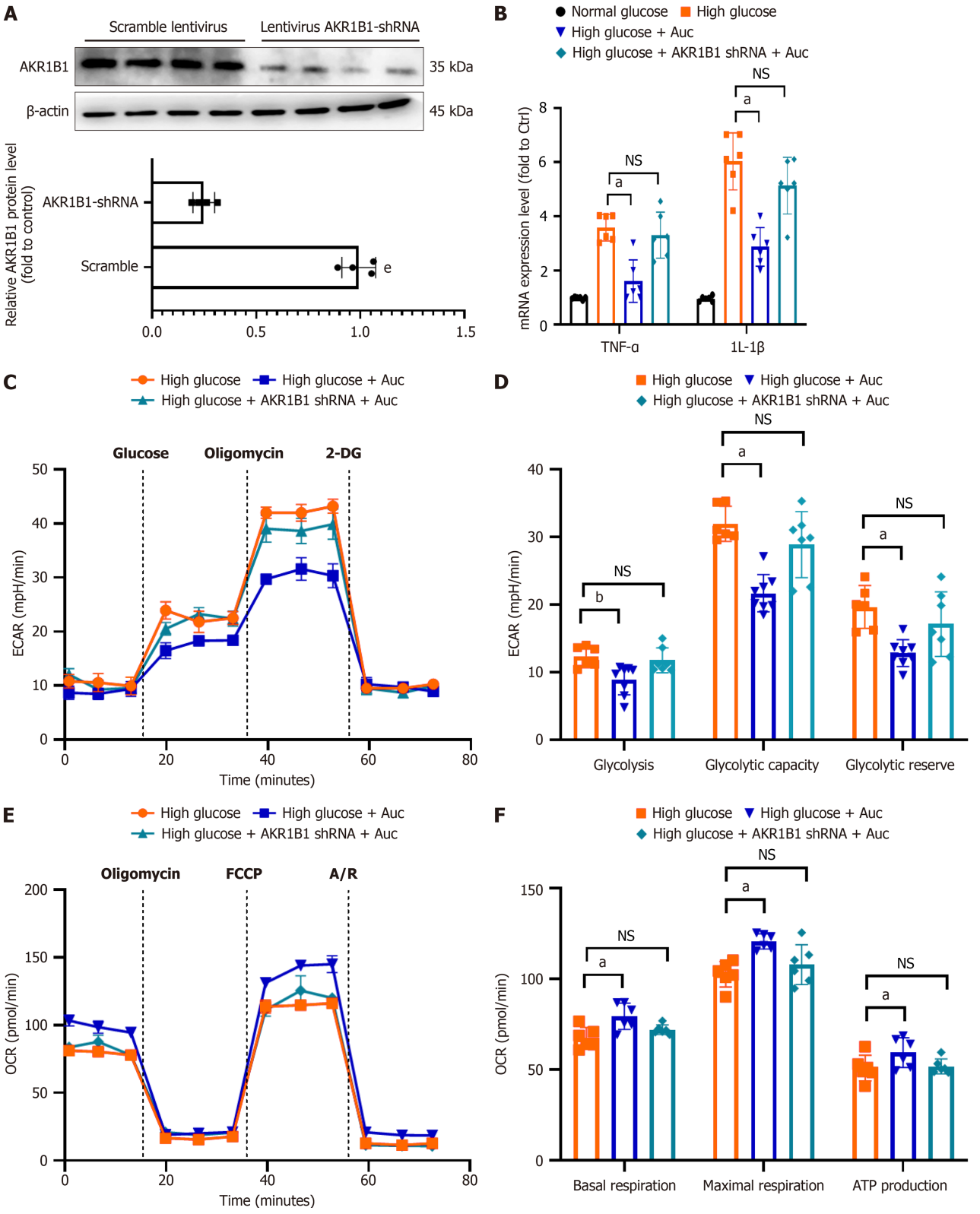

Figure 6 Aucubin fails to restore aerobic glycolysis and inflammation in the context of AKR1B1 deficiency. A: The expression level of AKR1B1 after transfecting AKR1B1 shRNA lentivirus. The quantitative analysis of the relative expression of AKR1B1 below. Data are expressed as mean ± SEM (n = 4); B: The mRNA levels of pro-inflammatory cytokine; C-F: The experimental program of extracellular acidification rate (C and D) and the oxygen consumption rate (E and F) of BV-2 measured by Seahorse XFe96 Extracellular Flux Analyzer. Data are expressed as mean ± SEM (n = 6). $^{a}P < 0.01$, $^{b}P < 0.05$, high glucose *vs* high glucose + aucubin. NS: No significance; Auc: Aucubin; 2-DG: 2-deoxy-d-glucose; ECAR: Extracellular acidification rate; OCR: Oxygen consumption rate.

[57]. Inhibitor-I was used to inhibit MMP-9, starting 2 days before and continuing 5 days post-injury, and delayed the onset of allodynia by at least 6 days. Daily intrathecal injections of a synthetic MMP-2 inhibitor (Inhibitor-III) reduced allodynia for up to 10 days[58].

Our study observed a significant increase in the mRNA levels of MMP-2 and MMP-9 in STZ-induced diabetic mice. Aucubin treatment ameliorated the elevated mRNA levels of MMP-2 following STZ administration. Western blotting confirmed increased MMP-2 expression in STZ-treated mice; however, aucubin did not decrease MMP-2 expression in these mice. While these data does not conclusively establish the role of MMPs in the effects of aucubin on DNP, further investigation into MMP-2 and MMP-9 inhibitors as potential therapeutic agents is warranted.

This study had some limitations. The impact of aucubin on other neuroinflammation animal models, such as complete freund's adjuvant-induced pain or LPS-induced pain *via* AKR1B1, was not observed. Further fundamental research should be conducted. Our results indicate that AKR1B1 may act as a potential target protein mediating the effects of aucubin. Cryo-electron microscopy to acquire high-resolution three-dimensional interaction structures between AKR1B1 and aucubin represents a promising avenue for further investigation. Approximately 370 clinical trials concerning painful diabetic neuropathies were listed on the clinicaltrials.gov website. Nevertheless, the impact of aucubin on painful diabetic neuropathies has not been determined. The clinical efficacy of aucubin necessitates further consideration.

The precise etiology of DNP remains incompletely understood. Aucubin, derived from natural medicine, shows significant promise in alleviating STZ-induced aerobic glycolysis and inflammation in DNP. The results of AKR1B1-shRNA lentivirus transfected in microglia cell lines highlight AKR1B1 as a potential target protein mediating the effects of aucubin.

CONCLUSION

This study provides a crucial theoretical foundation for developing new therapeutic approaches for DNP. Aucubin mitigates the elevation of microglial aerobic glycolysis and inflammation in DNP *via* aldose reductase.

ACKNOWLEDGEMENTS

Thanks for the technical support by the Core Facilities, Zhejiang University School of Medicine.

FOOTNOTES

Author contributions: Zheng XZ and Fang JS designed the study; Zheng XZ and Yu HY prepared the samples, performed the experiments, and analyzed the data; Chen YR and Fang JS wrote the original manuscript; all authors read and approved the final manuscript.

Supported by National Natural Science Foundation of China, No. 82001424.

Institutional animal care and use committee statement: All procedures involving animals were reviewed and approved by the Institutional Animal Care and Use Committee of the Zhejiang University Experimental Animal Ethics Committee Institutional Review Board (Approval No. ZJU20240012).

Conflict-of-interest statement: The authors declare that they have no known competing financial interests or personal relationships that could have appeared to influence the work reported in this paper.

Data sharing statement: The data generated in the present study may be requested from the corresponding author. The data generated in the present study are included in the figures and/or tables of this article.

ARRIVE guidelines statement: The authors have read the ARRIVE guidelines, and the manuscript was prepared and revised according to the ARRIVE guidelines.

Country of origin: China

ORCID number: Xue-Zhen Zheng 0009-0007-2045-9694; Ye-Ru Chen 0000-0002-2457-7854.

S-Editor: Lin C
L-Editor: A
P-Editor: Xu ZH

REFERENCES

1 **Rosenberger DC**, Blechschmidt V, Timmerman H, Wolff A, Treede RD. Challenges of neuropathic pain: focus on diabetic neuropathy. *J Neural Transm (Vienna)* 2020; **127**: 589-624 [PMID: 32036431 DOI: 10.1007/s00702-020-02145-7]

2 **Pop-Busui R**, Boulton AJ, Feldman EL, Bril V, Freeman R, Malik RA, Sosenko JM, Ziegler D. Diabetic Neuropathy: A Position Statement by the American Diabetes Association. *Diabetes Care* 2017; **40**: 136-154 [PMID: 27999003 DOI: 10.2337/dc16-2042]

3 **Callaghan BC**, Gallagher G, Fridman V, Feldman EL. Diabetic neuropathy: what does the future hold? *Diabetologia* 2020; **63**: 891-897 [PMID: 31974731 DOI: 10.1007/s00125-020-05085-9]

4 **Calcutt NA**. Diabetic neuropathy and neuropathic pain: a (con)fusion of pathogenic mechanisms? *Pain* 2020; **161**: S65-S86 [PMID: 32999525 DOI: 10.1097/j.pain.0000000000001922]

5 **Pop-Busui R**, Braffett BH, Wessells H, Herman WH, Martin CL, Jacobson AM, Sarma AV. Diabetic Peripheral Neuropathy and Urological Complications in Type 1 Diabetes: Findings From the Epidemiology of Diabetes Interventions and Complications Study. *Diabetes Care* 2022; **45**: 119-126 [PMID: 34728530 DOI: 10.2337/dc21-1276]

6 **Baskozos G**, Hébert HL, Pascal MM, Themistocleous AC, Macfarlane GJ, Wynick D, Bennett DL, Smith BH. Epidemiology of neuropathic pain: an analysis of prevalence and associated factors in UK Biobank. *Pain Rep* 2023; **8**: e1066 [PMID: 37090682 DOI: 10.1097/PR9.0000000000001066]

7 **Cheng SC**, Quintin J, Cramer RA, Shepardson KM, Saeed S, Kumar V, Giamarellos-Bourboulis EJ, Martens JH, Rao NA, Aghajanirefah A, Manjeri GR, Li Y, Ifrim DC, Arts RJ, van der Veer BM, Deen PM, Logie C, O'Neill LA, Willems P, van de Veerdonk FL, van der Meer JW, Ng A, Joosten LA, Wijmenga C, Stunnenberg HG, Xavier RJ, Netea MG. mTOR- and HIF-1α-mediated aerobic glycolysis as metabolic basis for trained immunity. *Science* 2014; **345**: 1250684 [PMID: 25258083 DOI: 10.1126/science.1250684]

8 **Rao J**, Wang H, Ni M, Wang Z, Wang Z, Wei S, Liu M, Wang P, Qiu J, Zhang L, Wu C, Shen H, Wang X, Cheng F, Lu L. FSTL1 promotes liver fibrosis by reprogramming macrophage function through modulating the intracellular function of PKM2. *Gut* 2022; **71**: 2539-2550 [PMID: 35140065 DOI: 10.1136/gutjnl-2021-325150]

9 **Lin Q**, Li K, Chen Y, Xie J, Wu C, Cui C, Deng B. Oxidative Stress in Diabetic Peripheral Neuropathy: Pathway and Mechanism-Based Treatment. *Mol Neurobiol* 2023; **60**: 4574-4594 [PMID: 37115404 DOI: 10.1007/s12035-023-03342-7]

10 **Banerjee S**. Aldo Keto Reductases AKR1B1 and AKR1B10 in Cancer: Molecular Mechanisms and Signaling Networks. *Adv Exp Med Biol* 2021; **1347**: 65-82 [PMID: 33945128 DOI: 10.1007/5584_2021_634]

11 **Zhao Q**, Han B, Wang L, Wu J, Wang S, Ren Z, Wang S, Yang H, Carbone M, Dong C, Melino G, Chen WL, Jia W. AKR1B1-dependent fructose metabolism enhances malignancy of cancer cells. *Cell Death Differ* 2024; **31**: 1611-1624 [PMID: 39406918 DOI: 10.1038/s41418-024-01393-4]

12 **Kallinikou D**, Tsentidis C, Kekou K, Katsalouli M, Louraki M, Kanaka-Gantenbein C, Kanavakis E, Karavanaki K. Homozygosity of the Z-2 polymorphic variant in the aldose reductase gene promoter confers increased risk for neuropathy in children and adolescents with Type 1 diabetes. *Pediatr Diabetes* 2022; **23**: 104-114 [PMID: 34773353 DOI: 10.1111/pedi.13285]

13 **Chalk C**, Benstead TJ, Moore F. Aldose reductase inhibitors for the treatment of diabetic polyneuropathy. *Cochrane Database Syst Rev* 2007; **2007**: CD004572 [PMID: 17943821 DOI: 10.1002/14651858.CD004572.pub2]

14 **Ramirez MA**, Borja NL. Epalrestat: an aldose reductase inhibitor for the treatment of diabetic neuropathy. *Pharmacotherapy* 2008; **28**: 646-655 [PMID: 18447661 DOI: 10.1592/phco.28.5.646]

15 **Vishwakarma VK**, Paswan SK, Arora T, Verma RK, Yadav HN. Pain Allaying Epalrestat-Loaded Lipid Nanoformulation for the Diabetic Neuropathic Pain Interventions: Design, Development, and Animal Study. *Curr Drug Metab* 2022; **23**: 571-583 [PMID: 35950248 DOI: 10.2174/1389200223666220810152633]

16 **Boyle J**, Eriksson ME, Gribble L, Gouni R, Johnsen S, Coppini DV, Kerr D. Randomized, placebo-controlled comparison of amitriptyline, duloxetine, and pregabalin in patients with chronic diabetic peripheral neuropathic pain: impact on pain, polysomnographic sleep, daytime functioning, and quality of life. *Diabetes Care* 2012; **35**: 2451-2458 [PMID: 22991449 DOI: 10.2337/dc12-0656]

17 **Yang P**, Zhang Q, Shen H, Bai X, Liu P, Zhang T. Research progress on the protective effects of aucubin in neurological diseases. *Pharm Biol* 2022; **60**: 1088-1094 [PMID: 35634723 DOI: 10.1080/13880209.2022.2074057]

18 **Yao D**, Wang Y, Chen Y, Chen G. The Analgesia Effect of Aucubin on CFA-Induced Inflammatory Pain by Inhibiting Glial Cells Activation-Mediated Inflammatory Response *via* Activating Mitophagy. *Pharmaceuticals (Basel)* 2023; **16** [PMID: 38004411 DOI: 10.3390/ph16111545]

19 **Xiao S**, Zhong N, Yang Q, Li A, Tong W, Zhang Y, Yao G, Wang S, Liu J, Liu Z. Aucubin promoted neuron functional recovery by suppressing inflammation and neuronal apoptosis in a spinal cord injury model. *Int Immunopharmacol* 2022; **111**: 109163 [PMID: 35994851 DOI: 10.1016/j.intimp.2022.109163]

20 **Wang H**, Zhou XM, Wu LY, Liu GJ, Xu WD, Zhang XS, Gao YY, Tao T, Zhou Y, Lu Y, Wang J, Deng CL, Zhuang Z, Hang CH, Li W. Aucubin alleviates oxidative stress and inflammation *via* Nrf2-mediated signaling activity in experimental traumatic brain injury. *J Neuroinflammation* 2020; **17**: 188 [PMID: 32539839 DOI: 10.1186/s12974-020-01863-9]

21 **Notartomaso S**, Scarselli P, Mascio G, Liberatore F, Mazzon E, Mammana S, Gugliandolo A, Cruccu G, Bruno V, Nicoletti F, Battaglia G. N-Acetylcysteine causes analgesia in a mouse model of painful diabetic neuropathy. *Mol Pain* 2020; **16**: 1744806920904292 [PMID: 32009537 DOI: 10.1177/1744806920904292]

22 **O'Brien PD**, Sakowski SA, Feldman EL. Mouse models of diabetic neuropathy. *ILAR J* 2014; **54**: 259-272 [PMID: 24615439 DOI: 10.1093/ilar/ilt052]

23 **Chaplan SR**, Bach FW, Pogrel JW, Chung JM, Yaksh TL. Quantitative assessment of tactile allodynia in the rat paw. *J Neurosci Methods* 1994; **53**: 55-63 [PMID: 7990513 DOI: 10.1016/0165-0270(94)90144-9]

24 **Zhang S**, Chen Y, Wang Y, Wang H, Yao D, Chen G. Tau Accumulation in the Spinal Cord Contributes to Chronic Inflammatory Pain by Upregulation of IL-1β and BDNF. *Neurosci Bull* 2024; **40**: 466-482 [PMID: 38148427 DOI: 10.1007/s12264-023-01152-4]

25 **Wang YT**, Lu K, Yao DD, Zhang SX, Chen G. Anti-inflammatory and analgesic effect of Forsythiaside B on complete Freund's adjuvant-induced inflammatory pain in mice. *Biochem Biophys Res Commun* 2023; **645**: 55-60 [PMID: 36680937 DOI: 10.1016/j.bbrc.2023.01.036]

26 **Wang YJ**, Liu MG, Wang JH, Cao W, Wu C, Wang ZY, Liu L, Yang F, Feng ZH, Sun L, Zhang F, Shen Y, Zhou YD, Zhuo M, Luo JH, Xu TL, Li XY. Restoration of Cingulate Long-Term Depression by Enhancing Non-apoptotic Caspase 3 Alleviates Peripheral Pain Hypersensitivity. *Cell Rep* 2020; **33**: 108369 [PMID: 33176141 DOI: 10.1016/j.celrep.2020.108369]

27 **Chen Y**, Zheng D, Wang H, Zhang S, Zhou Y, Ke X, Chen G. Lipocalin 2 in the Paraventricular Thalamic Nucleus Contributes to DSS-

Induced Depressive-Like Behaviors. *Neurosci Bull* 2023; **39**: 1263-1277 [PMID: 36920644 DOI: 10.1007/s12264-023-01047-4]

28 **Chen K**, Qi X, Zhu LL, Li ML, Cong B, Li YM. Quantitative analysis of microglia morphological changes in the hypothalamus of chronically stressed rats. *Brain Res Bull* 2024; **206**: 110861 [PMID: 38141789 DOI: 10.1016/j.brainresbull.2023.110861]

29 **Hu Y**, Mai W, Chen L, Cao K, Zhang B, Zhang Z, Liu Y, Lou H, Duan S, Gao Z. mTOR-mediated metabolic reprogramming shapes distinct microglia functions in response to lipopolysaccharide and ATP. *Glia* 2020; **68**: 1031-1045 [PMID: 31793691 DOI: 10.1002/glia.23760]

30 **Kim S**, Chen J, Cheng T, Gindulyte A, He J, He S, Li Q, Shoemaker BA, Thiessen PA, Yu B, Zaslavsky L, Zhang J, Bolton EE. PubChem 2023 update. *Nucleic Acids Res* 2023; **51**: D1373-D1380 [PMID: 36305812 DOI: 10.1093/nar/gkac956]

31 **Daina A**, Michielin O, Zoete V. SwissTargetPrediction: updated data and new features for efficient prediction of protein targets of small molecules. *Nucleic Acids Res* 2019; **47**: W357-W364 [PMID: 31106366 DOI: 10.1093/nar/gkz382]

32 **Stelzer G**, Rosen N, Plaschkes I, Zimmerman S, Twik M, Fishilevich S, Stein TI, Nudel R, Lieder I, Mazor Y, Kaplan S, Dahary D, Warshawsky D, Guan-Golan Y, Kohn A, Rappaport N, Safran M, Lancet D. The GeneCards Suite: From Gene Data Mining to Disease Genome Sequence Analyses. *Curr Protoc Bioinformatics* 2016; **54**: 1.30.1-1.30.33 [PMID: 27322403 DOI: 10.1002/cpbi.5]

33 **Szklarczyk D**, Kirsch R, Koutrouli M, Nastou K, Mehryary F, Hachilif R, Gable AL, Fang T, Doncheva NT, Pyysalo S, Bork P, Jensen LJ, von Mering C. The STRING database in 2023: protein-protein association networks and functional enrichment analyses for any sequenced genome of interest. *Nucleic Acids Res* 2023; **51**: D638-D646 [PMID: 36370105 DOI: 10.1093/nar/gkac1000]

34 **Shannon P**, Markiel A, Ozier O, Baliga NS, Wang JT, Ramage D, Amin N, Schwikowski B, Ideker T. Cytoscape: a software environment for integrated models of biomolecular interaction networks. *Genome Res* 2003; **13**: 2498-2504 [PMID: 14597658 DOI: 10.1101/gr.1239303]

35 **Wu T**, Hu E, Xu S, Chen M, Guo P, Dai Z, Feng T, Zhou L, Tang W, Zhan L, Fu X, Liu S, Bo X, Yu G. clusterProfiler 4.0: A universal enrichment tool for interpreting omics data. *Innovation (Camb)* 2021; **2**: 100141 [PMID: 34557778 DOI: 10.1016/j.xinn.2021.100141]

36 **Walter W**, Sánchez-Cabo F, Ricote M. GOplot: an R package for visually combining expression data with functional analysis. *Bioinformatics* 2015; **31**: 2912-2914 [PMID: 25964631 DOI: 10.1093/bioinformatics/btv300]

37 **Li X**, Wei S, Niu S, Ma X, Li H, Jing M, Zhao Y. Network pharmacology prediction and molecular docking-based strategy to explore the potential mechanism of Huanglian Jiedu Decoction against sepsis. *Comput Biol Med* 2022; **144**: 105389 [PMID: 35303581 DOI: 10.1016/j.compbiomed.2022.105389]

38 **Li C**, Pan J, Xu C, Jin Z, Chen X. A Preliminary Inquiry Into the Potential Mechanism of Huang-Lian-Jie-Du Decoction in Treating Rheumatoid Arthritis *via* Network Pharmacology and Molecular Docking. *Front Cell Dev Biol* 2021; **9**: 740266 [PMID: 35127697 DOI: 10.3389/fcell.2021.740266]

39 **Wang D**, Pan X, Zhou Y, Wu Z, Ren K, Liu H, Huang C, Yu Y, He T, Zhang X, Yang L, Zhang H, Han MH, Liu C, Cao JL, Yang C. Lateral septum-lateral hypothalamus circuit dysfunction in comorbid pain and anxiety. *Mol Psychiatry* 2023; **28**: 1090-1100 [PMID: 36642737 DOI: 10.1038/s41380-022-01922-y]

40 **Hu Q**, Cai H, Ke X, Wang H, Zheng D, Chen Y, Wang Y, Chen G. The lateral septum partakes the regulation of propofol-induced anxiety-like behavior. *Eur J Pharmacol* 2024; **977**: 176756 [PMID: 38897021 DOI: 10.1016/j.ejphar.2024.176756]

41 **Song ZH**, Song XJ, Yang CL, Cao P, Mao Y, Jin Y, Xu MY, Wang HT, Zhu X, Wang W, Zhang Z, Tao WJ. Up-regulation of microglial chemokine CXCL12 in anterior cingulate cortex mediates neuropathic pain in diabetic mice. *Acta Pharmacol Sin* 2023; **44**: 1337-1349 [PMID: 36697977 DOI: 10.1038/s41401-022-01046-7]

42 **Li Y**, Kong E, Ding R, Chu R, Lu J, Deng M, Hua T, Yang M, Wang H, Chen D, Song H, Wei H, Zhang P, Han C, Yuan H. Hyperglycemia-induced Sirt3 downregulation increases microglial aerobic glycolysis and inflammation in diabetic neuropathic pain pathogenesis. *CNS Neurosci Ther* 2024; **30**: e14913 [PMID: 39123294 DOI: 10.1111/cns.14913]

43 **Gao F**, Zheng ZM. Animal models of diabetic neuropathic pain. *Exp Clin Endocrinol Diabetes* 2014; **122**: 100-106 [PMID: 24554509 DOI: 10.1055/s-0033-1363234]

44 **Szkudelski T**. The mechanism of alloxan and streptozotocin action in B cells of the rat pancreas. *Physiol Res* 2001; **50**: 537-546 [PMID: 11829314]

45 **Fajrin FA**, Nugroho AE, Nurrochmad A, Susilowati R. Ginger extract and its compound, 6-shogaol, attenuates painful diabetic neuropathy in mice *via* reducing TRPV1 and NMDAR2B expressions in the spinal cord. *J Ethnopharmacol* 2020; **249**: 112396 [PMID: 31743763 DOI: 10.1016/j.jep.2019.112396]

46 **Zeng X**, Guo F, Ouyang D. A review of the pharmacology and toxicology of aucubin. *Fitoterapia* 2020; **140**: 104443 [PMID: 31790767 DOI: 10.1016/j.fitote.2019.104443]

47 **Xue HY**, Gao GZ, Lin QY, Jin LJ, Xu YP. Protective effects of aucubin on H_2O_2-induced apoptosis in PC12 cells. *Phytother Res* 2012; **26**: 369-374 [PMID: 21728203 DOI: 10.1002/ptr.3562]

48 **Chen S**, Zeng X, Zong W, Wang X, Chen L, Zhou L, Li C, Huang Q, Huang X, Zeng G, Hu K, Ouyang DS. Aucubin Alleviates Seizures Activity in Li-Pilocarpine-Induced Epileptic Mice: Involvement of Inhibition of Neuroinflammation and Regulation of Neurotransmission. *Neurochem Res* 2019; **44**: 472-484 [PMID: 30666488 DOI: 10.1007/s11064-018-2700-y]

49 **Xue HY**, Lu YN, Fang XM, Xu YP, Gao GZ, Jin LJ. Neuroprotective properties of aucubin in diabetic rats and diabetic encephalopathy rats. *Mol Biol Rep* 2012; **39**: 9311-9318 [PMID: 22810648 DOI: 10.1007/s11033-012-1730-9]

50 **Xue H**, Jin L, Jin L, Zhang P, Li D, Xia Y, Lu Y, Xu Y. Neuroprotection of aucubin in primary diabetic encephalopathy. *Sci China C Life Sci* 2008; **51**: 495-502 [PMID: 18488169 DOI: 10.1007/s11427-008-0069-x]

51 **Coelho AI**, Berry GT, Rubio-Gozalbo ME. Galactose metabolism and health. *Curr Opin Clin Nutr Metab Care* 2015; **18**: 422-427 [PMID: 26001656 DOI: 10.1097/MCO.0000000000000189]

52 **Shao MM**, Xiang HJ, Lu H, Yin PH, Li GW, Wang YM, Chen L, Chen QG, Zhao C, Lu Q, Wu T, Ji G. Candidate metabolite markers of peripheral neuropathy in Chinese patients with type 2 diabetes. *Am J Transl Res* 2022; **14**: 5420-5440 [PMID: 36105024]

53 **Kaur M**, Misra S, Swarnkar P, Patel P, Das Kurmi B, Das Gupta G, Singh A. Understanding the role of hyperglycemia and the molecular mechanism associated with diabetic neuropathy and possible therapeutic strategies. *Biochem Pharmacol* 2023; **215**: 115723 [PMID: 37536473 DOI: 10.1016/j.bcp.2023.115723]

54 **Saraswathy R**, Anand S, Kunnumpurath SK, Kurian RJ, Kaye AD, Vadivelu N. Chromosomal Aberrations and Exon 1 Mutation in the AKR1B1 Gene in Patients with Diabetic Neuropathy. *Ochsner J* 2014; **14**: 339-342 [PMID: 25249799]

55 **Krizkova S**, Zitka O, Masarik M, Adam V, Stiborova M, Eckschlager T, Hubalek J, Kizek R. Clinical importance of matrix metalloproteinases. *Bratisl Lek Listy* 2011; **112**: 435-440 [PMID: 21863613]

56 **Kuhad A**, Singh P, Chopra K. Matrix metalloproteinases: potential therapeutic target for diabetic neuropathic pain. *Expert Opin Ther Targets* 2015; **19**: 177-185 [PMID: 25243524 DOI: 10.1517/14728222.2014.960844]

57 **Chattopadhyay S**, Myers RR, Janes J, Shubayev V. Cytokine regulation of MMP-9 in peripheral glia: implications for pathological processes and pain in injured nerve. *Brain Behav Immun* 2007; **21**: 561-568 [PMID: 17189680 DOI: 10.1016/j.bbi.2006.10.015]

58 **Kobayashi H**, Chattopadhyay S, Kato K, Dolkas J, Kikuchi S, Myers RR, Shubayev VI. MMPs initiate Schwann cell-mediated MBP degradation and mechanical nociception after nerve damage. *Mol Cell Neurosci* 2008; **39**: 619-627 [PMID: 18817874 DOI: 10.1016/j.mcn.2008.08.008]

Published by **Baishideng Publishing Group Inc**
7041 Koll Center Parkway, Suite 160, Pleasanton, CA 94566, USA
Telephone: +1-925-3991568
E-mail: office@baishideng.com
Help Desk: https://www.f6publishing.com/helpdesk
https://www.wjgnet.com